

## Article

# A Comparison of the Tortuosity Phenomenon in Retinal Arteries and Veins Using Digital Image Processing and Statistical Methods

Sufian A. Badawi <sup>1,2,\*</sup> , Maen Takruri <sup>1</sup> , Djamel Guessoum <sup>3</sup> , Isam Elbadawi <sup>4</sup>, Ameera Albadawi <sup>5</sup> ,  
Ajay Nileshwar <sup>6,7</sup>  and Emad Mosalam <sup>8</sup> 

- <sup>1</sup> Center of Information, Communication and Networking Education and Innovation (ICONET), American University of Ras Al Khaimah, Ras Al Khaimah 72603, United Arab Emirates; maen.takruri@aurak.ac.ae
- <sup>2</sup> Department of Computing, National University of Sciences and Technology (NUST), Islamabad 44000, Pakistan
- <sup>3</sup> Electrical Engineering Department, Ecole de Technologie Supérieure, Montreal, QC H3C 1K3, Canada; djamel.guessoum.1@ens.etsmtl.ca
- <sup>4</sup> Industrial Engineering Department, College of Engineering, University of Ha'il, Ha'il 81481, Saudi Arabia; i.elbadawi@uoh.edu.sa
- <sup>5</sup> Department of Computer Science, College of Computing and Informatics, University of Sharjah, Sharjah P.O. Box 27272, United Arab Emirates; u22106819@sharjah.ac.ae
- <sup>6</sup> Department of Ophthalmology, RAK Medical, and Health Sciences University, Ras Al Khaimah 72603, United Arab Emirates; ajaykamath@rakhmsu.ac.ae
- <sup>7</sup> Ministry of Health and Prevention, Saqr Hospital, Ras Al Khaimah 72603, United Arab Emirates
- <sup>8</sup> Dr. Emad Musalam Eyes Clinic, Ras Al Khaimah P.O. Box 5450, United Arab Emirates; emadeyeyclinic@gmail.com
- \* Correspondence: t.sufianbadawi@aurak.ac.ae or sufian.badawi@seecs.edu.pk; Tel.: +971-563062104



**Citation:** Badawi, S.A.; Takruri, M.; Guessoum, D.; Elbadawi, I.; Albadawi, A.; Nileshwar, A.; Mosalam, E. A Comparison of the Tortuosity Phenomenon in Retinal Arteries and Veins Using Digital Image Processing and Statistical Methods. *Mathematics* **2023**, *11*, 3811. <https://doi.org/10.3390/math11183811>

Academic Editor: Shiao-fen Fang

Received: 27 July 2023

Revised: 22 August 2023

Accepted: 25 August 2023

Published: 5 September 2023



**Copyright:** © 2023 by the authors. Licensee MDPI, Basel, Switzerland. This article is an open access article distributed under the terms and conditions of the Creative Commons Attribution (CC BY) license (<https://creativecommons.org/licenses/by/4.0/>).

**Abstract:** The tortuosity of retinal blood vessels is an important phenomenon, and it can act as a biomarker in the diagnosis of several eye diseases. The study of abnormalities in the tortuosity of retinal arteries and veins provides ophthalmologists with important information for disease diagnosis. Our study aims to compare the tortuosity relation between retinal arteries and veins by quantifying the vessels' tortuosity in the retina using 14 tortuosity measures applied to the AV-classification retinal dataset. Two feature sets are created, one for arteries and the other for veins. The comparison between the tortuosity of arteries and veins is based on a two-sample *T*-test statistical method, a regression analysis between the quantified tortuosity features, principal component analysis at the dataset level, and the introduction of the arteriovenous length ratios concept to compare the variations in these new ratios to see the tortuosity behavior in each image. The methods' results have shown that the tortuosity of retinal arteries and veins is similar. The result of the two-sample *T*-test supports the research hypothesis, as the *P*-value obtained was greater than 0.05. Furthermore, the regression analysis between arteries and veins features showed a high correlation ( $r^2 = 89.39\%$  and  $89.11\%$ ) for arteries and veins, respectively. The study concludes that the retinal vessel type has no statistical significance in the tortuosity calculation results.

**Keywords:** retinal images; retinal blood vessels; skeletonization; tortuosity; inflection count metric; six sigma; linear regression analysis; two-sample *T*-test; principal component analysis; arteriovenous length ratio (AVLR)

**MSC:** 68U10; 92C55; 65D18

## 1. Introduction

The human retina fundus images, where the blood arteries and veins are readily visible, are crucial for identifying many eye illnesses and vessel morphology changes. It is also evident that the vessel morphological changes in the retinal vessels indicate the worsening

of eye diseases. For example, the twistedness and the vessel thickness changes are signals of eye disease severity such as diabetic retinopathy [1,2], hypertensive retinopathy [3], central retinal vein occlusion (CRVO) [4], retinopathy of prematurity (ROP) [5,6], systemic hypertension [7], and the plus disease. Tortuosity is also linked to gender, hypertension, aging, and other cardiovascular risk factors [8]. The tortuosity patterns as explained in [9] are as follows:

- Looping: when the vessel is S- or C-shaped with a multivessel symmetry sign.
- Coiling: when the vessel is chapped with a 360 deg turn in the vessel itself.
- Kinking: when it manifests arterial angulation in acute levels.

Many studies have reviewed and surveyed the tortuosity phenomenon. For example, in [10], the tortuosity measures have been grouped as curvature-based, distance-based, and a combination of the two, with a considerable description level of each algorithm and their formulas. The therapeutic use of the tortuosity measurements has been thoroughly evaluated by [11]. In contrast, Ref. [12] comprehensively analyzed the relationship between diabetic retinopathy and vascular tortuosity.

Several researchers have assessed and evaluated Tortuosity Metrics. For example, to calculate the length increase between two vessel points, Ref. [13] calculated the arc-to-chord ratio of a vessel segment. However, the drawback of this method is its insensitivity to the segment shape. The same approach was implemented in [14] and enhanced in [15,16] by applying a weighted scheme approach to ROP patients. The distance metric measure was enhanced by Grisan et al. [17], who improved the distance metric measure by considering the width of the curvature and the number of bends.

According to Wallace et al., [18], who used the ROP tool to a predefined array of pixels along the arteries and veins, the degree of tortuosity between two pixels is defined as the ratio of the length of the fragment curve divided by the length of the straightened curve joining these pixels. Although unaffected by the vessel's number of curve bends, this method is user-dependent.

It should be highlighted that the results of arc-to-chord-based tortuosity measuring methodologies must be more accurate since they are not sensitive to vessel fragments' morphological changes. Chandrinou et al.'s [19] study provided curvature-based tortuosity measure methodologies, in which the local average angle change approach is used, and the direction change of the segment curve is introduced. The method's drawback is that vessel branching with identical courses will not impact the tortuosity measurement. Integrals were used by Hart et al. [20] to determine the overall curvature; this approach is not sensitive to variations in the convexity of the vessel fragment curvature. On the other hand, Ref. [21] employed the pixels of the vessel fragment centerline and the addition of the second derivatives of the centerline coordinates. This method's performance relies on the vessel centerline's localization stage. When applied to type 1 diabetes cases, Ref. [22] defines tortuosity as the accumulation of angle changes throughout the length of a vessel, utilizing Hart's integral of the 'total square curvature (TSC)' in diabetes of type 1 [1]. In [23], a unique angle-variation-based tortuosity measure was developed using computer vision methods to extract the centerline of the image vessel tree and Gabor filters to segment the vessel tree and calculate the tortuosity using curvature metrics like the mean curvature by unit length and standard curvature deviation. The following works provide summaries of the hybrid tortuosity measures. Wavelet and fractal metrics were used in [24] to create a multiscale analysis tortuosity detection method. The vessel was estimated by Dougherty and Johnson [25] using a polynomial spline fitting. The precision of this method depends on the size of the data ball (dataset). The retinal vessel tortuosity level was calculated in [26,27] by building a resilient matrix based on the curvature and the chain coding scheme. This method requires the curvature k-value to be correctly determined. Chakravarty utilized a Quadratic Polynomial Decomposition, and Sivaswamy [28] utilized a Quadratic Polynomial Decomposition to create 'the tortuosity index (TI)'. The method can distinguish between the vessel bend's relative shape, orientation, and size, although their algorithm accuracy could have been better than the approach in [29].

By employing machine learning techniques, Ref. [30] suggested a technique that identifies the global tortuosity for clinical assessment. An eight-dimensions feature vector was initially generated by calculating the tortuosity and extracting the features after data processing. The top four features were then selected using a feature-selection technique based on the classification correlation. Finally, images from the databases were utilized to evaluate the performance of the approach. The highest sensitivity was provided by this method, which made use of the support vector machine (SVM) classifier. The feature selection approach also lowered the computational complexity and enhanced the overall sensitivity. Increased sensitivity was attained with this unique featured classifier. An observation noticed during the AV classification dataset preparation ignites this research's incentive: the arteries are tortuous in certain retinal images in the AV classification dataset. At the same time, the veins are normal, while in others, the veins are tortuous while the arteries are normal, and in other images, both the arteries and veins are tortuous or normal.

Although many studies measure the tortuosity of retinal vessels, no formula indicates if the tortuosity is in the arteries, veins, or both. This quantification represents a fresh area for future ophthalmic research, as it is studied for the first time in the field. Furthermore, the existing tortuosity calculation formulas in the literature generally measure tortuosity.

In this work, we investigated the tortuosity behavior difference between arteries and veins, and we assessed the tortuosity of all artery and vein segments in every retinal image (504 images) using the AV classification dataset. Then, we established formulas that statistically showed that, from a geometric aspect, the tortuosity of the arteries and veins are similar. The authors see this quantification as a unique area for future study on diagnosing pathological eye diseases related to arteries and veins using retinal image processing that will help give a clear path toward medical application.

This study aims to study the relationship between the arteries' and veins' tortuosity and address the research question, "Do the tortuosity metrics provide the same results if calculated for arteries or veins?"

Our strategy involves using 14 tortuosity measures on 504 colored retinal pictures from the AV classification database. These measures are applied to the arteries and veins. This formulates two feature sets, one for arteries and another for veins. Linear regression techniques and a two-sample *T*-test are used to support the research claim.

The main contributions of this work are as follows:

- Employs the optimized unsupervised machine learning method [31] to segment the vessels from the retina and deep learning to segment the arteries from the veins [32].
- Extracts the enhanced vessel segments using our approach in [33].
- The tortuosity is calculated using 14 measures for a large-scale AV classification dataset containing 504 retinal images with arteries and veins labels.
- Identifies the most strongly correlated components that reduced dimensionality via the correlation matrix and principal component analysis (PCA).
- A statistical hypothesis is introduced and statistically proved using two statistical methods: the two-sample *T*-test and linear regression models.
- A new arteriovenous length ratio (AVLR) is introduced to emphasize the above-concluded result at the image-level tortuosity.
- The research findings will help build an auto-diagnosing decision support system for localizing the tortuosity in arteries only, veins only, or even in one of the two eyes.

The remainder of this research work is composed of four main sections. Section 2 covers the creation of the materials and proposed methods to prove the research claim. Section 3 covers the results of the statistical techniques that proved the research claim. Finally, Sections 4 and 5 cover the discussions and the conclusion, respectively.

## 2. Methods and Materials

### 2.1. Materials

The authors used the AV classification dataset from [32]. The dataset is ideally suited for solving the challenges of vascular segmentation and AV classification, two forms of

retinal image processing using deep learning algorithms (see Figure 1). The 504 original colored images of fifty middle-aged participants were scanned using non-mydratic fundus cameras (Topcon) at a resolution of  $2002 \times 2000$  pixels to build the dataset, which was then labeled with two different types of ground truth information. The right and left eye images were both collected. There are limited publicly available datasets for experimenting with retinal image processing. These datasets, such as the DRIVE dataset (20 images), the STARE dataset (60 images), and the CHASEDB dataset (28 images), are very small. To address this issue, the AV classification dataset has been introduced. All 504 retinal images were used to calculate tortuosity metrics values for each vessel segment in the AV classification dataset images. Across 504 images, there were a total of 64,244 segments. The dataset is vast and can be utilized to assess any morphological transformations in a retinal image or observe other phenomena in the retinal vasculature.

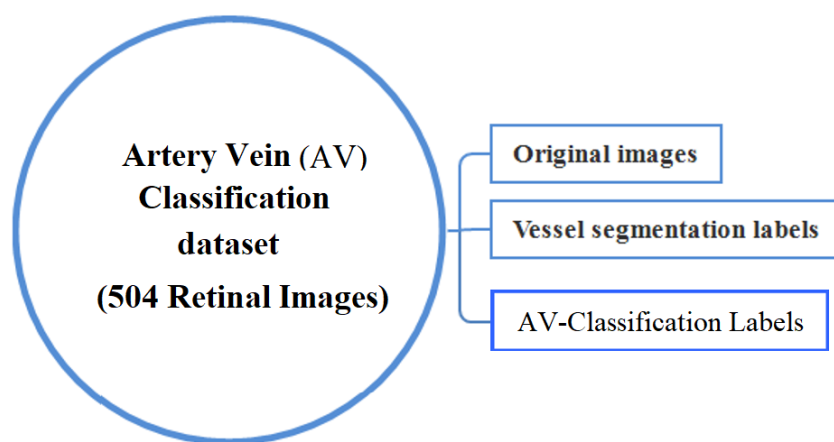


**Figure 1.** The AV classification dataset.

## 2.2. Method

In order to support the research claim, the approach in this study used statistical inferential analysis to calculate the tortuosity using 14 tortuosity measures and to create two feature sets, one for arteries and the other for veins. The specific methods are shown in Figure 2.

## 2.3. Feature Engineering

A row in the feature set was produced for each of the 504 photos in the materials dataset, as shown in Figure 3. An unsupervised machine learning method that classifies each pixel in a retinal image as a vessel pixel (white) or background pixel (black) is proposed [31]. This method uses a learned function, denoted as  $f()$ , which takes the grayscale color of the pixel as input and produces a binary output pixel  $y = f(x)$  that classifies each pixel whether it is in the vessel pixel or background pixel. We segmented the vasculature tree for each retinal image using [31]. In the black and white vessels segmented image, a process was conducted of iteratively thinning to skeletonize the vascular tree. The vessel segments were extracted after the intersection/bifurcation points were found, where each vessel fragment linked to two endpoints or intersection/bifurcation points in the skeleton. Each vessel segment was classified as an artery or vein segment using a deep learning method that utilized a fully connected convolutional neural network [32]. The deep neural network consisted of 96 internal deep layers that enhanced the model's performance. The learned model took the pixel of the retinal image as input and classified it as either Artery, Vein, or background. The output pixel  $y = g(x)$  was obtained using a learned function,  $g()$ , which takes the pixel color as input and produces a colored output pixel (red for the artery, blue for the vein, and yellow for the background).

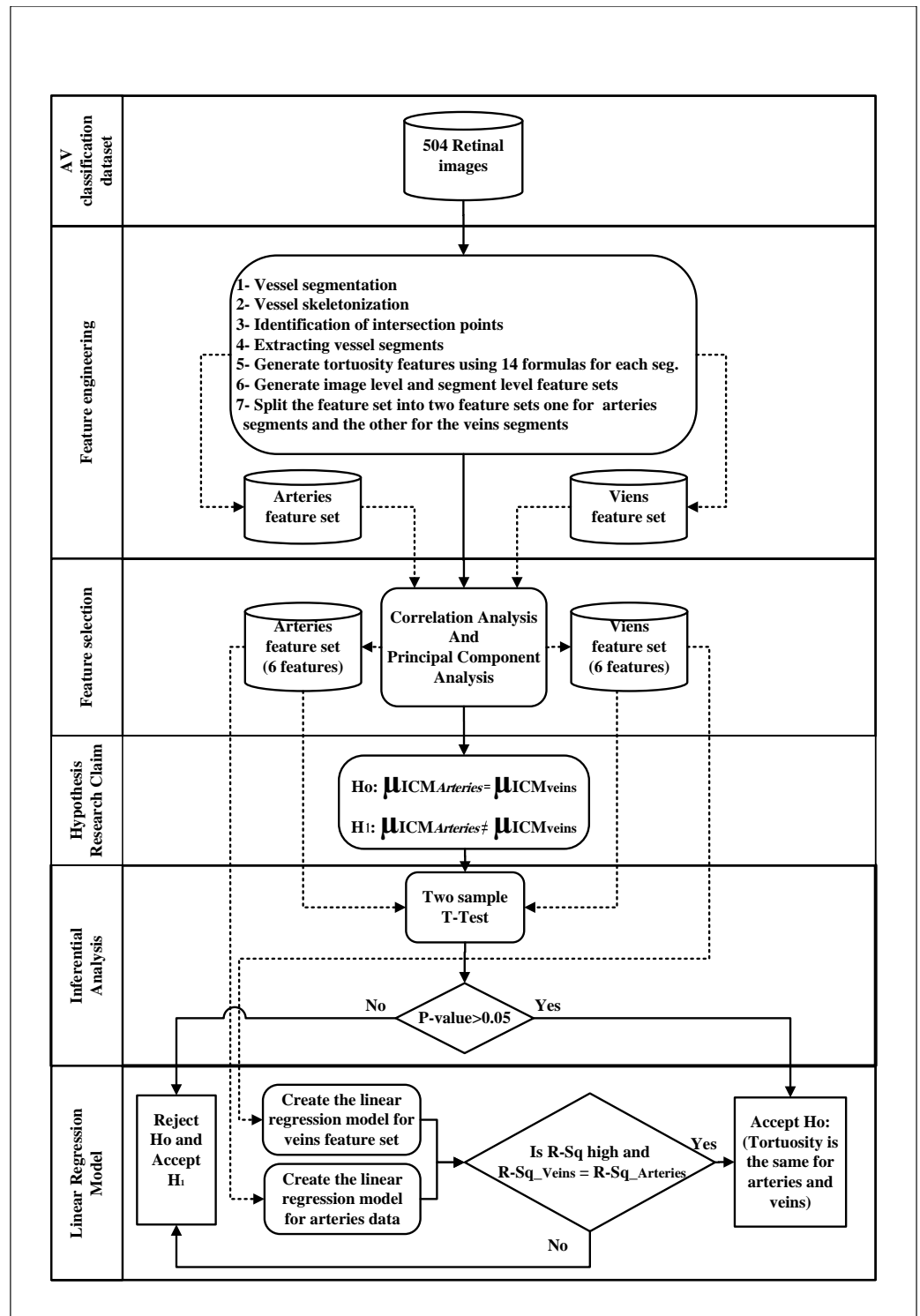


Figure 2. The method workflow.

The fourteen tortuosity Formula (1) through (14) shown in Table 1 were used to compute the vessel tortuosity for each vessel segment for each vessel fragment retrieved from the retina. The resulting features of each vessel segment were added to the feature set. The description of each tortuosity measure is summarized in Table 1.

**Table 1.** Tortuosity metrics used in the feature set.

| Metric Measure Description   | Equation   |
|--|--|
| <b>Chord:</b> The shortest distance between the two segments ends $(a_1, b_1)$ , $(a_2, b_2)$ .  | $Chord = \sqrt{(a_2 - a_1)^2 + (b_2 - b_1)^2}$ (1)                                     |
| <b>Arc:</b> The maximum non-infinite quasi-Euclidean spacing between the two ends of the segment’s centerline skeleton, the arc-length separating between the segment’s endpoints, the Separation in terms of the geodesics.                         | $d(\gamma(t_2) - \gamma(t_1)) = v *  t_2 - t_1 $ (2)                                   |
| <b>Distance Metric (DM):</b> The ratio of dividing the arc over chord. It is the most common measure in the scientific literature [34].  | $DM = \frac{Arc}{Chord}$ (3)   |
| <b>Tortuosity density (TD):</b> The sum is computed by splitting the segment into sub-segments and selecting sample points (n).  | $TD = \frac{n - 1}{n} \frac{1}{Arc} \sum_{i=1}^n [\frac{Lcs_i}{Lxs_i} - 1]$ (4)        |
| <b>The curvature at point p(a,b):</b>  | $C(p) = \frac{a'(p) * b''(p) - b'(p) * a''(p)}{(a'(p)^2 + b'(p)^2)^{\frac{3}{2}}}$ (5) |
| $\tau_1$ : Characterized by TD-1.  | $\tau_1 = TD - 1$ (6)  |
| $\tau_2$ : Integral sum of $C(p)$ .  | $\tau_2 = \int_{t_0}^{t_n} C(p) dt$ (7)  |
| $\tau_3$ : Integral sum of $C(p)^2$  | $\tau_3 = \int_{t_0}^{t_n} C(p)^2 dt$ (8)  |
| $\tau_4$ : Integral sum of $C(p) / Arc$  | $\tau_4 = \int_{t_0}^{t_n} \frac{C(p)}{Arc} dt$ (9)                                    |
| $\tau_5$ : Integral sum of $\frac{C(p)}{Arc}$  | $\tau_5 = \int_{t_0}^{t_n} \frac{C(p)^2}{Chord} dt$ (10)                               |
| $\tau_6$ : Integral sum of $C(p) / Chordlength$  | $\tau_6 = \int_{t_0}^{t_n} \frac{C(p)}{Chord} dt$ (11)                                 |
| $\tau_7$ : Integral sum of $C(p) * C(p) / Chordlength$   | $\tau_7 = \int_{t_0}^{t_n} \frac{C(p)^2}{Chord} dt$ (12)                               |
| <b>SOAM:</b> The summation of the angles between the two vectors created by three segment points at the segment skeleton in succession. The length of the segment is used to obtain the normalized sum of these orientations along the segment [34]. | $SOAM = \sum_{i=1}^n \frac{(180 - \alpha_i)}{Arc}$ (13)                                |
| <b>ICM:</b> The multiplication of the segment’s inflection points count by the distance metric.  | $ICM = (Inflection\_points + 1) * \frac{Arc}{Chord}$ (14)                              |

In the feature set that contains the 14 tortuosity measures calculated for the vessel segment, the results of those computations are inserted as a line. After creating image-wise tortuosity summary statistics to complete the images-level feature set, quantified tortuosity measurements were computed for each vessel segment based on the results to complete the fragment-wise feature set (see Figure 4).

**Tortuosity Metrics and Feature Set Preparation**

The features extracted for each segment were the straight-line distance, the geodesic distance, and a collection of other distance- and curvature-based tortuosity measurements.

The ERD diagram in Figure 4 shows the tables where the details of the images and their segments are recorded. Two feature sets were formed, one at the segment level and the other at the image level.

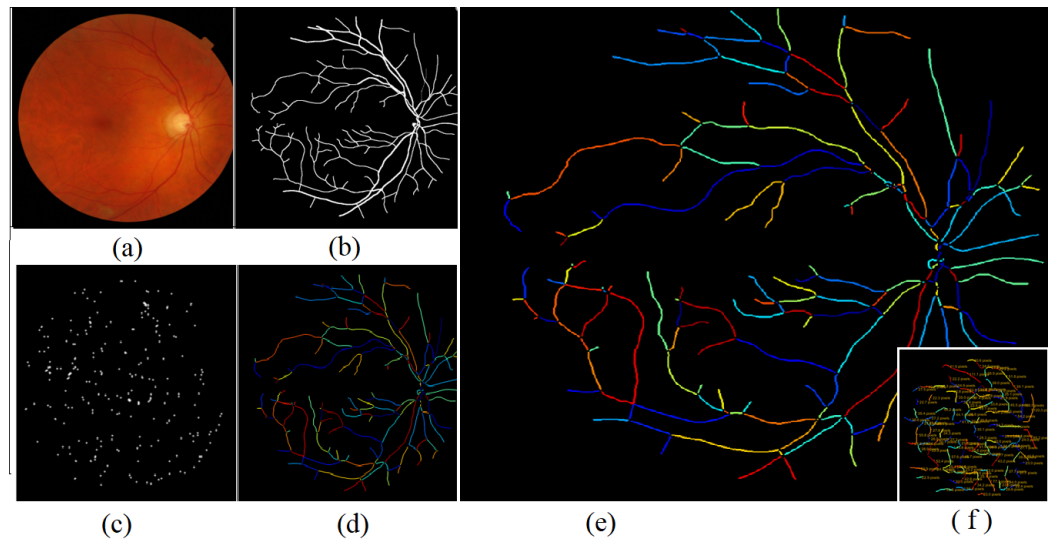


**Figure 3.** Snapshot of the retinal image at each step: (a) the colored retina; (b) the segmented vessels; (c) cross-section/branching points removal; (d) the vasculature tree skeleton; (e) vessel fragments; (f) calculation of vessel tortuosity.

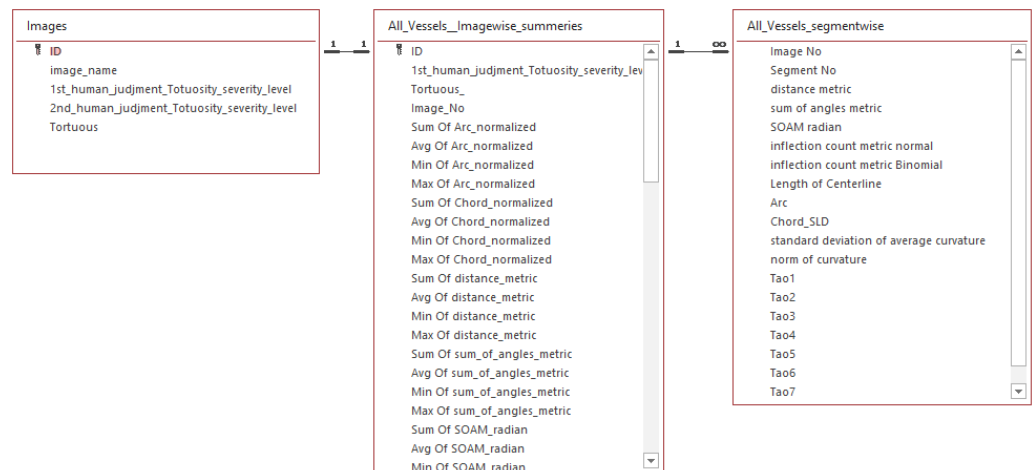


**Figure 4.** Entity relationship diagram for the generated features. It displays three prepared feature sets, which can be viewed as three Excel sheets or tables. The first table contains the names of all 504 retinal images, while the second table provides image-wise statistical summaries (Min, Max, Average, sum) of each tortuosity metric for each image (with 504 rows in total), which comprises 76 columns. The third table contains segment-wise statistical details. To view a sample of the segment-wise table data, please see the results section. These three tables are filled separately for arteries and veins, with the same Tortuosity metrics calculations are applied to both.

Figure 5 visually represents a few tortuosity metrics. The tortuosity attributes for each vessel are intended to be recorded in a record that will establish a row for each fragment in the segment-level feature set. Each image’s totals were summed and grouped to form the imagewise summaries.

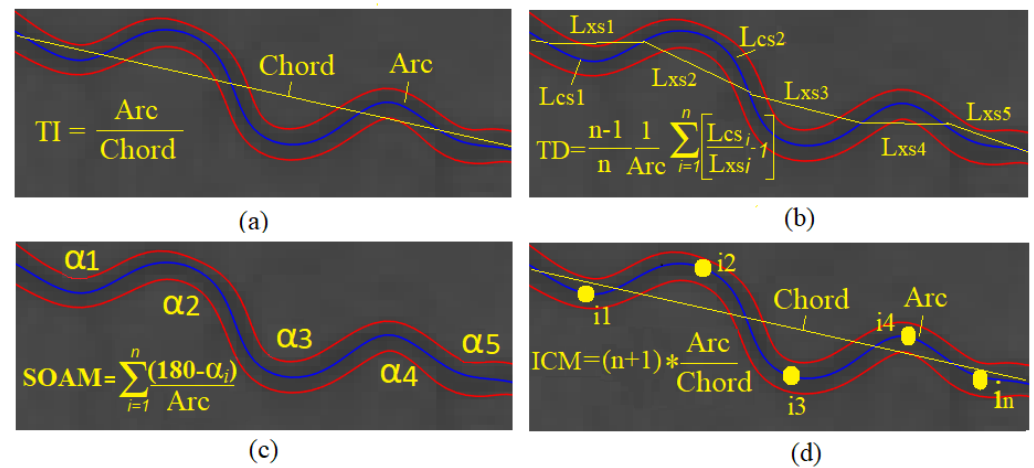


**Figure 5.** Visualization of four tortuosity metrics: (a) Tortuosity-index or Distance Metric; (b) Tortuosity-density; (c) SOAM; (d) ICM.

2.4. Feature Selection

Feature selection was achieved using correlation analysis and principal component analysis.

2.4.1. Correlation Analysis

The correlation analysis is used as a statistical method to find the relationship significance and strength between two variables [35]. The equation used in our study is 'Pearson's Product-Moment Correlation [36] for calculating the correlation coefficient (15).

$$\rho_{ab} = \frac{n \sum a_i b_i - \sum a_i \sum b_i}{\sqrt{(n \sum a_i^2 - (\sum a_i)^2)} \sqrt{(n \sum b_i^2 - (\sum b_i)^2)}} \tag{15}$$

The closer the correlation coefficient result is to (1) or (-1), the stronger the increasing or decreasing relationship between the variables, respectively [36]. Hence, the research question that the correlation is examining here is as follows: Is there a statistically significant difference between *Tortuosity\_Metric\_a* results when the segment is an artery and when the same segment is a vein?

2.4.2. Principal Component Analysis

PCA is a linear dimensionality reduction method that operates in an unsupervised manner. Its objective is to reduce the number of variables that are correlated with each other to a smaller number of independent variables without losing its impact on the dependent variables and effectively capture the primary causes of variability present within the dataset. It provides an overview of linear relationships between inputs and variables and visualizes this linear relationship (Note: visualized in Section 3.2).

The technique is extensively employed for the purpose of feature extraction and data compression, and it can also serve as a valuable tool for exploratory data analysis or as a preliminary step in the application of machine learning algorithms. The components that emerge from the analysis are ordered based on the extent to which they account for the variance in the data. These components can be employed for data visualization, interpretation, clustering, or classification. In this research work case, after having it ordered, the top six components were used to reduce the tortuosity metrics to the top six and verify it with the correlation results to confirm the dimensionality reduction and features finally selected that contribute to building the regression formulas.

### 2.5. Hypothesis Research Claim

By employing inferential analysis and hypothesis testing, we derived the research null hypothesis and its alternative hypothesis as follows:

$$H_0 : \mu_{ICM_{Arteries}} = \mu_{ICM_{veins}} \quad (16)$$

$$H_1 : \mu_{ICM_{Arteries}} \neq \mu_{ICM_{veins}} \quad (17)$$

where  $\mu_{ICM_{Arteries}}$  and  $\mu_{ICM_{veins}}$  are the average results of 'Inflection\_count\_metric\_Normal' of the vein fragments and artery fragments, respectively.

We are checking that there is no significant difference in the means of the arteries  $\mu_{ICM_{Arteries}}$  and veins  $\mu_{ICM_{veins}}$  datasets. In a Two-sample  $T$ -test, the null hypothesis is always the claim that the means are equivalent, while the alternative hypothesis claims otherwise. This way, the null hypothesis is accepted if the  $p$ -value is greater than the critical value (0.05); otherwise, the null hypothesis is rejected [37].

Aiming to find the optimal tortuosity measure, we have calculated the correlation matrix that measures the significant mutual relationship between every two measures to identify which measure has the dominant tortuosity features of the others. That characterizes the highest tortuosity phenomena in the retinal vasculature. This statistical analysis identified the top two tortuosity measures and the optimal set of other correlated measures. This helped in selecting the highest correlated six tortuosity metrics to be selected to proceed in the analysis.

### 2.6. The Research Question

To find the answer to the research question: "Is there a difference in tortuosity behavior between arteries and veins?" the authors split the segment-wise feature set into two sets. The first contained the artery segments' tortuosity-features details, and the second contained the vein segments' tortuosity-features details.

The research question is answered using 1—linear regression, 2—two sample  $T$ -test, 3—principal component analysis (PCA), 4—correlation analysis, and 5—the introduction of arteriovenous length ratio.

Through PCA and correlation analysis, dimensionality reduction was achieved, which helped identify the six highest correlated tortuosity metrics out of the total of fourteen. These metrics were then used in the following analysis steps. The regression analysis was performed on each feature set to find the tortuosity formula of each feature set and to compare the R-Sq values. Likewise, the two-sample  $T$ -test was performed on the two feature sets. The first sample contained the 'Inflection count metric normal' values for arteries records, and the second contained the 'Inflection count metric normal' for veins records.

### 2.7. Image-Level Statistical Analysis for Tortuosity Behavior between Arteries and Veins

In one retinal image of a specific patient, the tortuosity may appear in arteries alone, veins alone, or both. On the other hand, if there is no tortuosity, the vessels branch smoothly from the optic disc until the smallest vessel branch appears in the retina. The tortuosity shape is generally similar to arteries and veins when it occurs. To compare the tortuosity behavior of arteries and veins at the image level, averaging summaries were collected for all artery segments, and the same was applied to vein segments to generate the formulas in Table 2.

Formulas (18) and (19) were generated to study the characteristics of the ratio of artery length to vein length for each image of the AV classification dataset. Similarly, Formulas (20)–(26) were generated to study the characteristics of the mean tortuosity metric for the arteries over the same mean tortuosity metric for the veins ( $DM$ ,  $ICM$ ,  $ICMb$ ,  $SOAM$ ,  $CL$ ,  $NC$ , and  $SDAC$ ) for each image of the AV classification dataset.

**Table 2.** Introduced Arteriovenous Length Ratios.

| Introduced Length Ratio Description  | Equation  |
|--|---|
| <b>Arteriovenous Chord Length Ratio:</b> The ratio of all arteries’ mean Euclidean distance over all veins’ mean Euclidean distance in the retinal image.  | $AV\_Chord\_Length\_Ratio = \frac{Mean(Artery\_Chord\_Length)}{Mean(Vein\_Chord\_Length)} \quad (18)$ |
| <b>Arteriovenous Arc Length Ratio:</b> The ratio of the mean geodesic distance of all arteries over the mean geodesic distance of all veins in the retinal image.  | $AV\_Arc\_Length\_Ratio = \frac{Mean(Artery\_Arc\_Length)}{Mean(Vein\_Arc\_Length)} \quad (19)$       |
| <b>Arteriovenous Distance Metric Ratio:</b> The ratio of all arteries’ mean tortuosity distance metric over the mean tortuosity distance metric of all veins in the retinal image.   | $AV\_DM\_Length\_Ratio = \frac{Mean(Artery\_DM\_Length)}{Mean(Vein\_DM\_Length)} \quad (20)$          |
| <b>Arteriovenous Inflection Count Metric Ratio:</b> The ratio of the mean tortuosity Inflection Count Metric of all arteries over the mean tortuosity Inflection Count Metric of all veins in the retinal image.                             | $AV\_ICM\_Length\_Ratio = \frac{Mean(Artery\_ICM\_Length)}{Mean(Vein\_ICM\_Length)} \quad (21)$       |
| <b>Arteriovenous Inflection Count Metric Binomial Ratio:</b> The ratio of the mean tortuosity Inflection Count Metric Binomial of all arteries over the mean tortuosity Inflection Count Metric Binomial of all veins in the retinal image.  | $AV\_ICMb\_Length\_Ratio = \frac{Mean(Artery\_ICMb\_Length)}{Mean(Vein\_ICMb\_Length)} \quad (22)$    |
| <b>Arteriovenous Sum of Angles Metric Ratio:</b> The ratio of the mean tortuosity Sum of Angles metric of all arteries over the mean tortuosity Sum of Angles metric of all veins in the retinal image.                                      | $AV\_SOAM\_Length\_Ratio = \frac{Mean(Artery\_SOAM\_Length)}{Mean(Vein\_SOAM\_Length)} \quad (23)$    |
| <b>Arteriovenous Norm of Curvature Ratio:</b> The mean of the curvature of all artery segments over the mean curvature of all vein segments in the retinal image.  | $AV\_NC\_Length\_Ratio = \frac{Mean(Artery\_NC\_Length)}{Mean(Vein\_NC\_Length)} \quad (24)$          |
| <b>Arteriovenous of Standard Deviation of Average curvature Ratio:</b> The ratio of the average-curvature standard deviation of all arteries over the mean of average curvature of the standard deviation of all veins in the retinal image. | $AV\_SDAC\_Length\_Ratio = \frac{Mean(Artery\_SDAC\_Length)}{Mean(Vein\_SDAC\_Length)} \quad (25)$    |
| <b>Arteriovenous of Centerline Length Ratio:</b> The ratio of the mean Centerline Length of all arteries over the mean Centerline Length of all veins in the retinal image.  | $AV\_CL\_Length\_Ratio = \frac{Mean(Artery\_CL\_Length)}{Mean(Vein\_CL\_Length)} \quad (26)$          |

Those ratios should be normally distributed and within the accepted range when the retinal image is healthy. Meanwhile, for a specific image, such formulas will vary to above or below the mean of the measure for all the vessel segments in the image if there is a tortuosity in the retinal veins alone or the retinal arteries alone.

### 3. Results

By generating the tortuosity feature set of the calculated fourteen tortuosity measures (see Table 3), it becomes possible to analyze this feature set to answer the research questions and statistically prove the similarity of the tortuosity phenomena for arteries versus veins. The feature set is split into two subsets, one for arteries and the other for veins.

#### 3.1. Feature Selection Using Correlation Analysis/Principal Component Analysis

The feature selection, dimensionality reduction, and analysis of the generated feature set’s tortuosity measures were performed by a correlation study and principal component analysis (PCA) to determine and visualize the relations between the features.

In the Table 4 correlation matrix values, each cell represents the correlation  $\rho_{xy}$  between the corresponding row feature x and column feature y. It represents high significance whenever the values are close to 1 or (−1).

**Table 3.** Sample segments tortuosity results.

| Image No. | Seg. No. | 1-A 2-V | Arc    | Chord  | DM     | SOAM   | ICMn   | ICMb   | SDavc  | Navc   | $\tau_1$ | $\tau_2$ | $\tau_3$ | $\tau_4$ | $\tau_5$ | $\tau_6$ | $\tau_7$ |
|-----------|----------|---------|--------|--------|--------|--------|--------|--------|--------|--------|----------|----------|----------|----------|----------|----------|----------|
| 2         | 42       | 2       | 0.1200 | 0.0900 | 0.0001 | 0.1300 | 0.0007 | 0.0008 | 0.0100 | 0.0014 | 0.0006   | 0.0100   | 0.0003   | 0.1200   | 0.1000   | 0.0050   | 0.0000   |
| 2         | 44       | 2       | 0.1800 | 0.1400 | 0.0002 | 0.3600 | 0.0011 | 0.0009 | 0.0100 | 0.0022 | 0.0011   | 0.0100   | 0.0001   | 0.1200   | 0.1000   | 0.0050   | 0.0000   |
| 2         | 46       | 2       | 0.0600 | 0.0400 | 0.0002 | 0.1300 | 0.0003 | 0.0002 | 0.0100 | 0.0009 | 0.0014   | 0.0800   | 0.0500   | 0.2500   | 0.3000   | 0.0090   | 0.0040   |
| 3         | 2        | 2       | 0.0800 | 0.0500 | 0.0002 | 0.1900 | 0.0002 | 0.0003 | 0.0200 | 0.0015 | 0.0011   | 0.0100   | 0.0001   | 0.1200   | 0.1000   | 0.0050   | 0.0000   |
| 3         | 4        | 2       | 0.3200 | 0.2700 | 0.0009 | 0.1300 | 0.0024 | 0.0024 | 0.1000 | 0.0041 | 0.0020   | 0.1400   | 0.1400   | 0.1700   | 0.2000   | 0.0060   | 0.0020   |
| 3         | 5        | 1       | 0.0200 | 0.0100 | 0.0002 | 0.0800 | 0.0001 | 0.0002 | 0.0100 | 0.0004 | 0.0009   | 0.0100   | 0.0001   | 0.1200   | 0.1000   | 0.0050   | 0.0000   |
| 44        | 117      | 1       | 0.2000 | 0.1600 | 0.0012 | 0.0800 | 0.0008 | 0.0012 | 0.0100 | 0.0021 | 0.0017   | 0.2600   | 0.2600   | 0.2800   | 0.3000   | 0.0100   | 0.0050   |
| 44        | 119      | 1       | 0.0030 | 0.0073 | 0.0300 | 0.0100 | 0.0011 | 0.0005 | 0.0059 | 0.0001 | 0.0700   | 0.0700   | 0.0600   | 0.5300   | 0.5000   | 0.0600   | 0.0600   |
| 45        | 1        | 1       | 0.1000 | 0.0700 | 0.0001 | 0.1300 | 0.0006 | 0.0006 | 0.0100 | 0.0014 | 0.0009   | 0.0100   | 0.0003   | 0.1200   | 0.1000   | 0.0050   | 0.0040   |
| 45        | 2        | 2       | 0.0078 | 0.0076 | 0.0200 | 0.0200 | 0.0020 | 0.0008 | 0.1400 | 0.0017 | 0.0200   | 0.0400   | 0.0200   | 0.3200   | 0.3000   | 0.0100   | 0.0100   |
| 45        | 3        | 1       | 0.0200 | 0.0100 | 0.0011 | 0.2500 | 0.0005 | 0.0004 | 0.0300 | 0.0011 | 0.0015   | 0.0100   | 0.0004   | 0.1300   | 0.1000   | 0.0050   | 0.0000   |
| 45        | 4        | 2       | 0.0200 | 0.0079 | 0.0002 | 0.0500 | 0.0000 | 0.0000 | 0.0200 | 0.0004 | 0.0012   | 0.0100   | 0.0000   | 0.1100   | 0.1000   | 0.0050   | 0.0000   |

Note: See the abbreviations list on Table 1.

**Table 4.** Correlation matrix for the fourteen tortuosity measures.

|  |       |       |       |       |       |       |       |       |      |       |      |      |      |      |      |      |      |  |
|--|-------|-------|-------|-------|-------|-------|-------|-------|------|-------|------|------|------|------|------|------|------|--|
| (1) vessel type                          | 1.00  |       |       |       |       |       |       |       |      |       |      |      |      |      |      |      |      |  |
| (2) Chord normalized                     | 0.00  | 1.00  |       |       |       |       |       |       |      |       |      |      |      |      |      |      |      |  |
| (3) distance metric                      | 0.00  | 0.15  | 1.00  |       |       |       |       |       |      |       |      |      |      |      |      |      |      |  |
| (4) SOAM                                 | −0.01 | 0.48  | −0.23 | 1.00  |       |       |       |       |      |       |      |      |      |      |      |      |      |  |
| (5) SOAM radian                          | −0.01 | 0.48  | −0.23 | 1.00  | 1.00  |       |       |       |      |       |      |      |      |      |      |      |      |  |
| (6) inflection count metric normal       | 0.00  | 0.44  | 0.78  | −0.09 | −0.09 | 1.00  |       |       |      |       |      |      |      |      |      |      |      |  |
| (7) inflection count metric Binomial     | 0.00  | 0.24  | 0.52  | −0.04 | −0.04 | 0.71  | 1.00  |       |      |       |      |      |      |      |      |      |      |  |
| (8) Centerline length (ARC normalized)   | 0.00  | 0.30  | 0.71  | −0.10 | −0.10 | 0.86  | 0.77  | 1.00  |      |       |      |      |      |      |      |      |      |  |
| (9) standard deviation of curvature mean | 0.00  | 0.11  | 0.53  | −0.24 | −0.24 | 0.40  | 0.24  | 0.38  | 1.00 |       |      |      |      |      |      |      |      |  |
| (10) normalized curvature                | 0.00  | 0.19  | 0.56  | −0.05 | −0.05 | 0.72  | 0.41  | 0.60  | 0.60 | 1.00  |      |      |      |      |      |      |      |  |
| (11) $\tau_1$                            | 0.00  | −0.02 | 0.34  | −0.15 | −0.15 | 0.10  | 0.06  | 0.08  | 0.15 | 0.06  | 1    |      |      |      |      |      |      |  |
| (12) $\tau_2$                            | 0.00  | 0.03  | 0.12  | −0.14 | −0.14 | 0.05  | 0.03  | 0.05  | 0.11 | 0.04  | 0.10 | 1.00 |      |      |      |      |      |  |
| (13) $\tau_3$                            | 0.00  | 0.04  | 0.12  | −0.13 | −0.13 | 0.05  | 0.04  | 0.06  | 0.12 | 0.04  | 0.10 | 0.98 | 1.00 |      |      |      |      |  |
| (14) $\tau_4$                            | 0.00  | −0.11 | 0.06  | −0.19 | −0.19 | −0.01 | −0.01 | −0.01 | 0.05 | −0.01 | 0.17 | 0.71 | 0.69 | 1.00 |      |      |      |  |
| (15) $\tau_5$                            | 0.00  | −0.11 | 0.06  | −0.19 | −0.19 | −0.01 | −0.01 | −0.01 | 0.05 | −0.01 | 0.17 | 0.71 | 0.69 | 1.00 | 1.00 |      |      |  |
| (16) $\tau_6$                            | 0.00  | −0.04 | 0.09  | −0.07 | −0.07 | 0.00  | 0.00  | 0.00  | 0.02 | 0.00  | 0.51 | 0.25 | 0.24 | 0.40 | 0.40 | 1.00 |      |  |
| (17) $\tau_7$                            | 0.00  | −0.05 | 0.09  | −0.09 | −0.09 | 0.00  | 0.00  | 0.00  | 0.03 | 0.00  | 0.51 | 0.30 | 0.30 | 0.46 | 0.46 | 0.99 | 1    |  |
| ↑Tortuosity Metrics→                     | (1)   | (2)   | (3)   | (4)   | (5)   | (6)   | (7)   | (8)   | (9)  | (10)  | (11) | (12) | (13) | (14) | (15) | (16) | (17) |  |

Note: The arrows indicate that the numbers in the last row correspond to tortuosity metrics in the first column.

The PCA is an approach used to reduce the dimensionality where the top representative components with high variance are selected, and the rest are ignored. In our case, the first six dimensions are the strongly correlated tortuosity metrics after being converted to a normal distribution (Box–Cox transformed). The correlation matrix in Table 4 shows that the ‘*Inflection count metric normal*’ feature is highly correlated with the five features ‘*Inflection count metric Binomial*’, ‘*Centerline length*’, ‘*Norm of curvature*’, ‘*Distance metric*’, and ‘*Chord normalized*’. On the other hand, the ‘*Distance metric*’ is highly correlated with the ‘*Inflection count metric normal*’, ‘*Inflection count metric Binomial*’, ‘*Centerline-length*’, and ‘*Norm of curvature*’. Similarly, using the principle component analysis, the same six metrics are identified among the 14 tortuosity metrics as they are the highest correlated. All the above six highly correlated features are selected from the two arteries and veins tortuosity feature sets, while the rest of the features are eliminated.

The results of the regression analysis performed on the feature sets via Minitab and the generated residual plots showed an R-squared of 89.11% for the veins and 89.39% for the arteries (refer to Figures 6 and 7). These results indicate that the vessel type is not a significant factor impacting the tortuosity measures, and they match the previous correlation matrix in Table 4. Column (4) shows that  $\rho_{xy}$  equals 0 or is very close to zero, indicating the non-existence of any linearity or significant relationship between the vessel type feature and the other analyzed tortuosity metrics.

**Arteries Segments Tortuosity Regression Equation**

$$\begin{aligned} \text{Inflection\_count\_metric\_normal} = & -0.00697 - 0.0834 \text{ Chord\_normalized} \\ & + 0.2219 \text{ Distance\_metric} \\ & + 0.1264 \text{ Inflection\_count\_metric\_Binomial} \\ & + 0.7997 \text{ Centerline\_Length} \\ & - 0.0484 \text{ Standard\_deviation\_of\_average\_curvature} \\ & + 0.3191 \text{ Norm\_of\_curvature} \end{aligned}$$

**Coefficients**

| Term                            | Coef     | SE Coef | T-Value | P-Value | VIF  |
|---------------------------------|----------|---------|---------|---------|------|
| Constant                        | -0.00697 | 0.00385 | -1.81   | 0.071   |      |
| Chord_normalized                | -0.0834  | 0.0118  | -7.09   | 0.000   | 1.93 |
| distance_metric                 | 0.2219   | 0.0319  | 6.96    | 0.000   | 2.82 |
| inflection_count_metric_Binomia | 0.1264   | 0.0307  | 4.12    | 0.000   | 4.08 |
| Centerline_Length               | 0.7997   | 0.0456  | 17.52   | 0.000   | 7.06 |
| standard_deviation_of_average_c | -0.0484  | 0.0168  | -2.88   | 0.004   | 1.86 |
| norm_of_curvature               | 0.3191   | 0.0488  | 6.54    | 0.000   | 2.83 |

**Model Summary**

| S         | R-sq   | R-sq(adj) | R-sq(pred) |
|-----------|--------|-----------|------------|
| 0.0296417 | 89.39% | 89.26%    | 87.90%     |

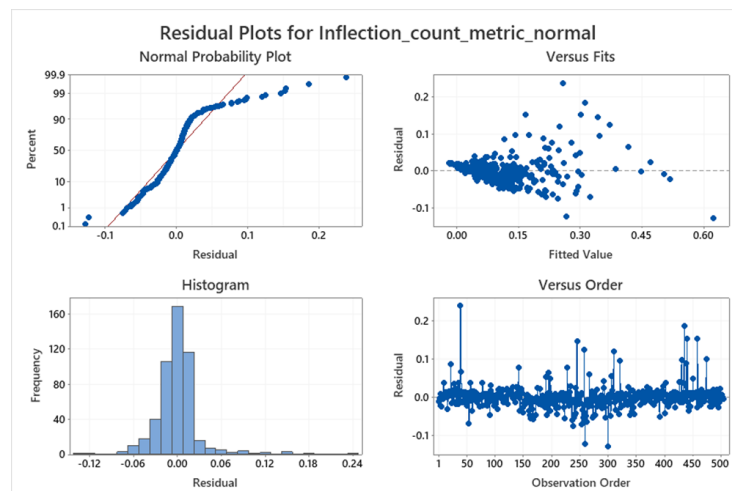


**Figure 6.** Artery segments linear regression analysis results for tortuosity metrics data taken from all the AV classification dataset images. Regression analysis Minitab output and the residual plots.

### Veins segments tortuosity Regression Equation

$$\begin{aligned} \text{Inflection\_count\_metric\_normal} = & -0.00938 - 0.1051 \text{ Chord\_normalized} \\ & + 0.3418 \text{ Distance\_metric} \\ & + 0.2353 \text{ Inflection\_count\_metric\_Binomia} \\ & + 0.5731 \text{ Centerline\_Length} \\ & - 0.1730 \text{ Standard\_deviation\_of\_average\_curvature} \\ & + 0.7979 \text{ Norm\_of\_curvature} \end{aligned}$$

### Predictors

| Term                            | Coef     | SE Coef | T-Value | P-Value | VIF  |
|---------------------------------|----------|---------|---------|---------|------|
| Constant                        | -0.00938 | 0.00415 | -2.26   | 0.024   |      |
| Chord_normalized                | -0.1051  | 0.0148  | -7.08   | 0.000   | 2.59 |
| Distance_metric                 | 0.3418   | 0.0323  | 10.58   | 0.000   | 3.09 |
| Inflection_count_metric_Binomia | 0.2353   | 0.0411  | 5.72    | 0.000   | 4.04 |
| Centerline_Length               | 0.5731   | 0.0496  | 11.56   | 0.000   | 6.21 |
| Standard_deviation_of_average_c | -0.1730  | 0.0206  | -8.38   | 0.000   | 1.94 |
| Norm_of_curvature               | 0.7979   | 0.0602  | 13.25   | 0.000   | 3.60 |

### Model Summary

| S         | R-sq   | R-sq(adj) | R-sq(pred) |
|-----------|--------|-----------|------------|
| 0.0321245 | 89.11% | 88.98%    | 87.22%     |

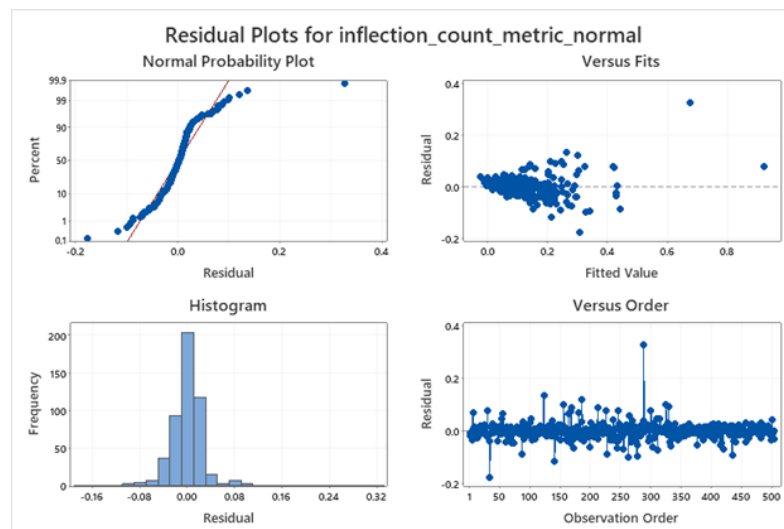


**Figure 7.** Vein segments linear regression analysis results for tortuosity metrics data taken from all the AV classification dataset images, Minitab output for regression analysis, and the residual plots.

The two composite formulas to calculate tortuosity are very similar, with high R-Sq 89.39% and 89.12%, indicating a strong correlation between the right-hand side variables and the left-hand side of each tortuosity equation. Furthermore, both show that the regression model strongly explains the tortuosity behavior regarding ICM, whether the segment is an artery or vein. The two-sample *T*-test further statistically supports those findings in the next experiment.

#### 3.1.1. Linear Regression Analysis

Linear regression analysis was performed for the 'Inflection count metric normal' with the highest correlated metrics columns (Inflection count metric binomial, length of centerline, norm of curvature, and the standard deviation of average curvature). Minitab statistical tool [38] was used for this analysis. The analysis was repeated twice, once for the artery segments and the second for the veins segments, to check whether the vessel type significantly impacts the tortuosity.

#### 3.1.2. Two Sample *T*-test

Two sample *T*-test was applied on the two samples for the arteries and the veins data: the 'Inflection count metric normal' ( $ICM_{arteries}$ ) column data of artery segments

vs. ‘Inflection count metric normal’ ( $ICM_{veins}$ ) for vein segments for all the images in the AV classification dataset. The research null and alternative hypotheses are  $H_0$  and  $H_1$  in Equations (16) and (17).

The research claim states, "when measuring the tortuosity ( $H_0$ ), ophthalmologists will achieve almost equivalent results in measuring the tortuosity for arteries versus measuring the tortuosity for veins".

The two sample  $T$ -test was applied in Minitab on the arteries’ and veins’ ‘inflection count metric normal’ columns. Figure 8 illustrates a box plot that clearly shows the similarity in the tortuosity results for arteries and veins. Finally, to validate the research claim, the authors checked the results of the two-sample  $T$ -test and reported the  $P\_value = 0.701$ . As  $P\_value$  is greater than 0.05, the null hypothesis  $H_0$  is accepted, implying no difference between the average  $ICM_{arteries}$  and the average  $ICM_{veins}$ . This implies that the research claim is proven.

**Method**

$\mu_1$ : population mean of Inflection\_count\_metric\_normal\_Arteries  
 $\mu_2$ : population mean of inflection\_count\_metric\_normal\_Veins  
 Difference:  $\mu_1 - \mu_2$

**Descriptive Statistics**

| Sample                                  | N   | Mean   | StDev  | SE Mean |
|---|-----|--------|--------|---------|
| Inflection_count_metric_normal_Arteries | 504 | 0.0926 | 0.0904 | 0.0040  |
| inflection_count_metric_normal_Veins    | 504 | 0.0903 | 0.0968 | 0.0043  |

**Estimation for Difference**

| Difference | 95% CI for Difference |
|------------|-----------------------|
| 0.00227    | (-0.00931, 0.01385)   |

**Test**

Null hypothesis  $H_0: \mu_1 - \mu_2 = 0$   
 Alternative hypothesis  $H_1: \mu_1 - \mu_2 \neq 0$

| T-Value | DF   | P-Value |
|---------|------|---------|
| 0.38    | 1001 | 0.701   |

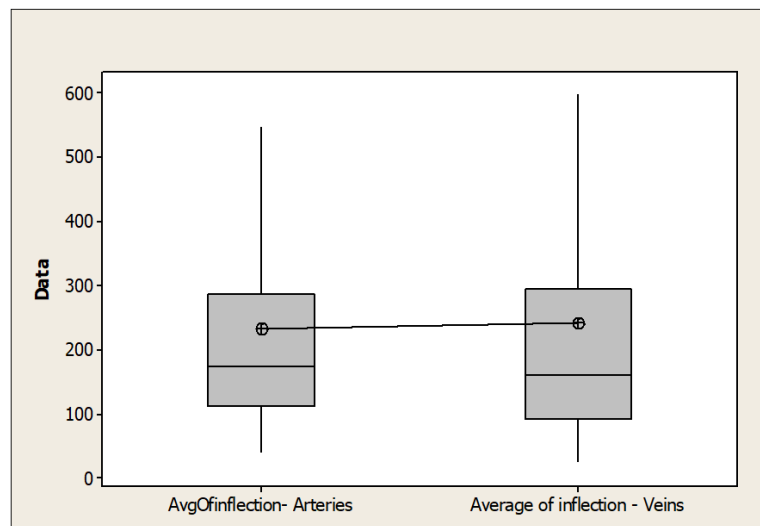


**Figure 8.** Two sample  $T$ -test results of avgofICM-arteries and avgofICM-veins for artery segments vs. vein segments in all the AV classification dataset images. The Minitab two sample  $T$ -test analysis output and the box plot for AvgofICM-arteries vs. AvgofICM-veins box plots.

**3.2. Visual Representation of the Linear Regression Using Dimensionality Reduction**

To visualize the regression tortuosity equations for arteries and veins on a two-dimensional plot, PCA was used to map five tortuosity variables at the right-hand side

of the tortuosity equation to one variable. It is named the “Principal component of five tortuosity metrics, and the resulting principal component of the five tortuosity metrics” and is plotted in Figures 6 and 7. PCA was used as it is commonly used for dimensionality reduction. For example, Figure 9 illustrates both regression formulas in one plot using the PCA and the regression plot. The five variables were collectively correlated to represent the data 100% in the generated one principal component data, which was used eventually as the vector of the x-axis in Figures 9 and 10.

**Eigenanalysis of the Correlation Matrix**

|            |        |        |        |        |        |
|------------|--------|--------|--------|--------|--------|
| Eigenvalue | 3.3788 | 0.8563 | 0.3971 | 0.2597 | 0.1081 |
| Proportion | 0.676  | 0.171  | 0.079  | 0.052  | 0.022  |
| Cumulative | 0.676  | 0.847  | 0.926  | 0.978  | 1.000  |

**Eigenvectors**

| Variable                                | PC1   |
|---|-------|
| Distance_metric                         | 0.457 |
| Inflection_count_metric_Binomia         | 0.464 |
| Length_of_Centerline                    | 0.489 |
| Standard_deviation_of_average_curvature | 0.339 |
| Norm_of_curvature                       | 0.471 |

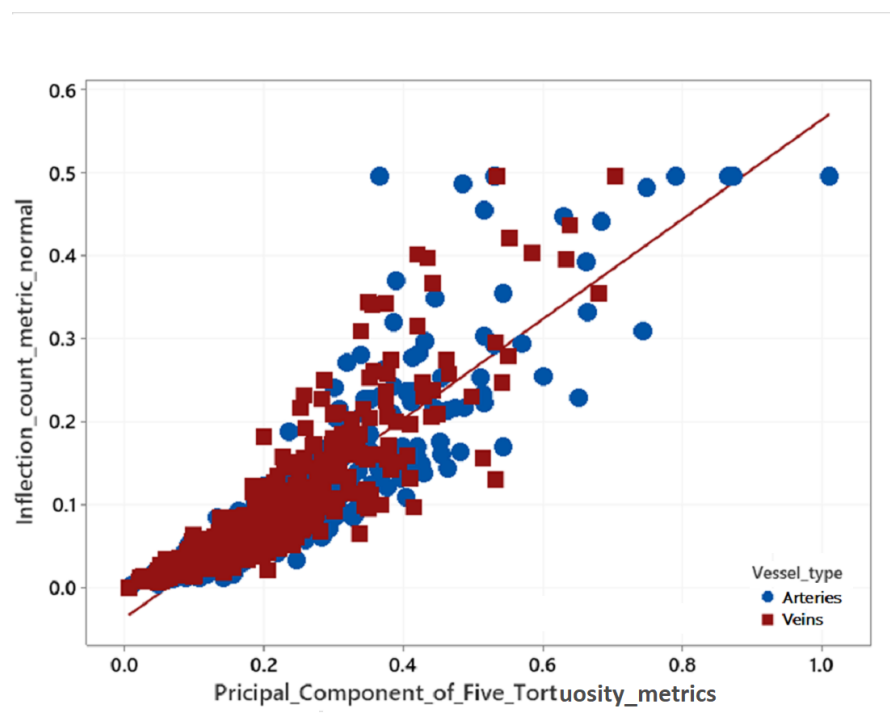


**Figure 9.** Illustration of the regression line plot for the arteries tortuosity data points where the arteries are represented in blue circles and the veins are represented as red squares (PCA linearity visualization).

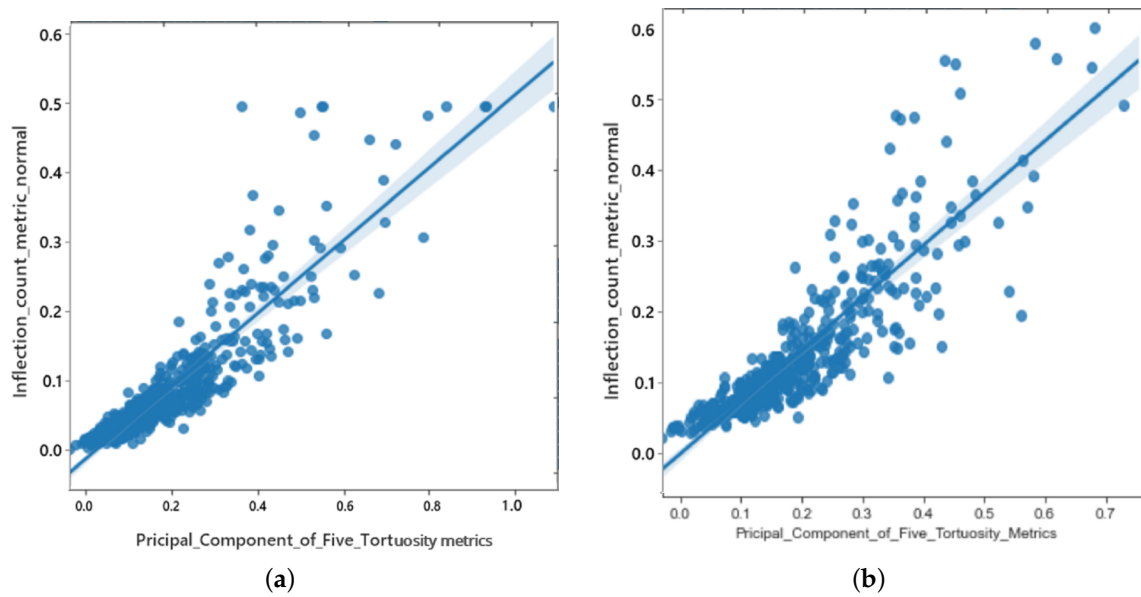


**Figure 10.** Regression line plot for (a) arteries and (b) veins data that predicts the tortuosity in terms of inflection count metric normal from one principle component derived from the five metrics: Distance metric, Inflection count metric Binomial, Length of Centerline, Standard deviation of average curvature, and Normal curvature.

### 3.3. Image-Level Arteriovenous Length Ratios Analysis

Arteries are thinner than veins [38]. It is known that arteries may become tortuous earlier than veins in some patients’ retinas (See Figure 11). However, if tortuosity happens, it will manifest in either the arteries, veins, or both. Nevertheless, in all of them, the possible twistedness shapes have the same morphological manifestation in both arteries and veins.

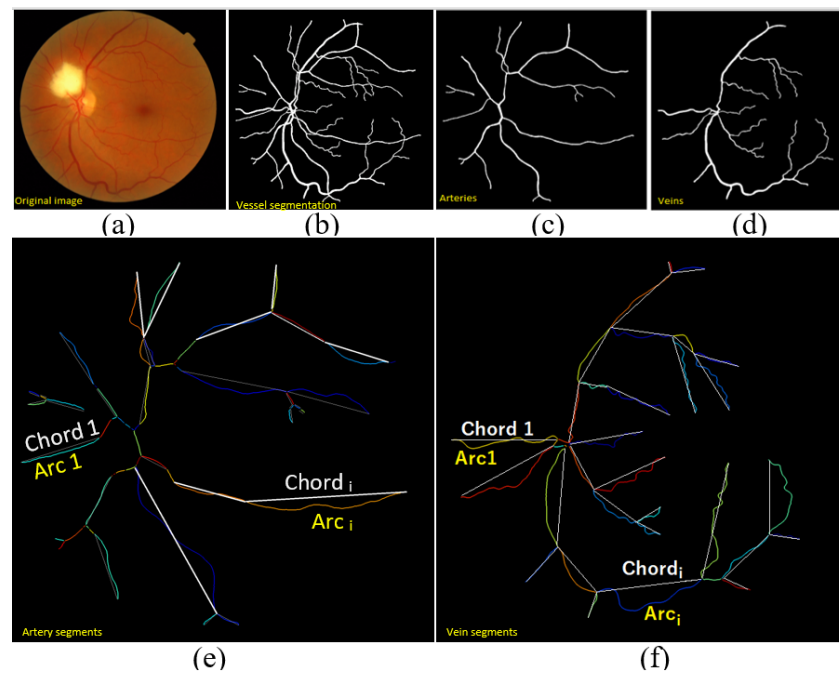


**Figure 11.** Visualization of the stages to extract the arc and the chord segments to calculate the arteriovenous length ratios formulas. (a) Original image, (b) vessels segmentation, (c) arteries, (d) veins, (e) arteries segments that are measured by arc or chord length, (f) veins segments that are measured by arc or chord length, for each image in AV classification dataset.

This fact emphasizes the above statistical conclusions, and to further analyze this arteriovenous tortuosity artery–vein relation, we calculate those ratios image-wise across the 504 images in the AV classification dataset. For each image, the arteriovenous chord length ratio in Equation (18) and arteriovenous arc length ratio in Equation (19) are generated in addition to the ratio of the mean of retinal arteries tortuosity metric over the mean of retinal veins tortuosity metric for each of the following tortuosity formulas (SOAM, ICM, ICMb, DM, CL, SDAC, NC).

Figure 12 shows two box plots of the vessel length ratios, one for the arc length ratio, which is the arteries' mean arc length divided by the veins' mean arc length, and the chord length ratio, which is the arteries mean chord length divided by the veins mean chord length. Those two ratios attribute each image in the AV classification dataset of the mean length of the arteries compared to the mean length of the veins in this specific retina. This identifies the healthiness of the vessels, whether they are tortuous or not, and how severe the deviation can be noticed in each fundus image of the AV classification dataset from those two ratios.

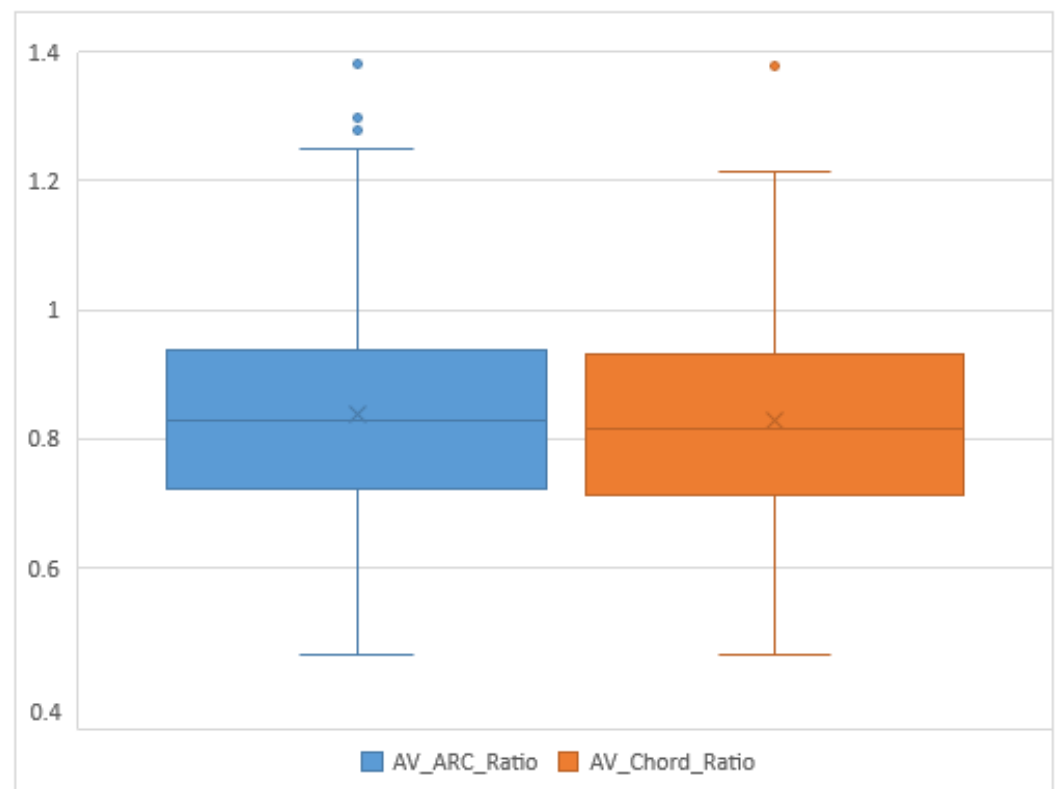


**Figure 12.** Box plot of arteriovenous arc length ratio and arteriovenous chord length ratio for each image in the AV classification dataset.

The box plot in Figure 12 shows that the arteriovenous chord length ratio (18) and arteriovenous arc length ratio (19) are normally distributed for all the 504 images in the AV classification dataset. The following facts can be concluded:

- As the distributions of the two box plots are comparable, both ratios show the same tortuosity behavior for artery length relative to vein length. These data support the statistical conclusion that the morphological behavior of tortuosity in arteries and veins is the same.
- The median is the straight line in the center of both box plots with a value of around, while the mean is the 'x' symbol in the plot immediately above the median with a value of 0.83. It implies that the average arc length of the artery is shorter than the average arc length of the vein. As the artery is narrower than the vein, it is less likely to present itself at the retinal surface.

- When both arteries and veins grow tortuous, their lengths rise. Hence, the ratio should equal 1. However, we can infer why the median diverged from 1 to 0.82 based on the fact of the difference in the width of the artery compared to the width of the vein and its relationship to being less apparent at the retinal surface, which was discussed before.
- Whenever the mean length of the arteries is greater than the mean length of the veins, the ratio deviates to the top portion of the box plot. The greater the length difference, the more the retinal image point above the median appears in the box plot. Fifty percent of the data from the normally distributed plot are of this kind.
- Whenever the mean length of both arteries is less than that of both veins, the ratio deviates to the bottom portion of the box plot. The more the length difference reduces, the more the retinal image point below the median appears in the box plot. In addition, based on the normal distribution plot, 50% of the data are of this kind.
- As both ratios exhibited a normal distribution, the arc and chord lengths may be utilized interchangeably to determine the nature of the discrepancy between the artery and vein lengths.

The box plot in Figure 13 shows that the arteriovenous tortuosity ratios in (20)–(26) are skewed right away from (above) the mean and median for some images in the AV classification dataset. We can conclude the following facts:

- The arteriovenous SOAM ratio is regularly distributed with a mean of 1 and a median of 1. This demonstrates how the curvature angle influences the computation and maintains the results inside the y-axis's narrow range by causing numbers to oscillate between 0 and 360. Nevertheless, since the y-axis range is so small, it may not reveal any possible differences between arteries and veins.
- When both arteries and veins have the same degree of tortuosity, both lengths rise, and the ratio approaches 1. In AV SOAM Ratio and AV SDAC Ratio, the mean and median are 1, whereas the rest of the tortuosity ratios have medians and means between 1 and 0.7. Once again, this deviation can be explained by the difference in the artery's width compared to the vein's width and its relationship to being more apparent on the retinal surface in each image.
- Whenever the mean length of arteries exceeds the mean length of veins, the ratio deviates to the top portion of the box plot. The greater the length difference, the higher above the median the retinal image point is reflected in the box plot. The tortuosity metric ratios are skewed towards the arteries, suggesting that the arteries in the retinal picture are much more tortuous than the veins.
- Whenever the mean length of both arteries is less than that of both veins, the ratio deviates to the bottom portion of the box plot. The greater the length difference, the more the retinal image point below the median is reflected in the box plot. In the box plots shown in Figure 13, the vein tortuosity does not differ significantly from the median, showing fewer instances in which vein tortuosity appears in veins alone.

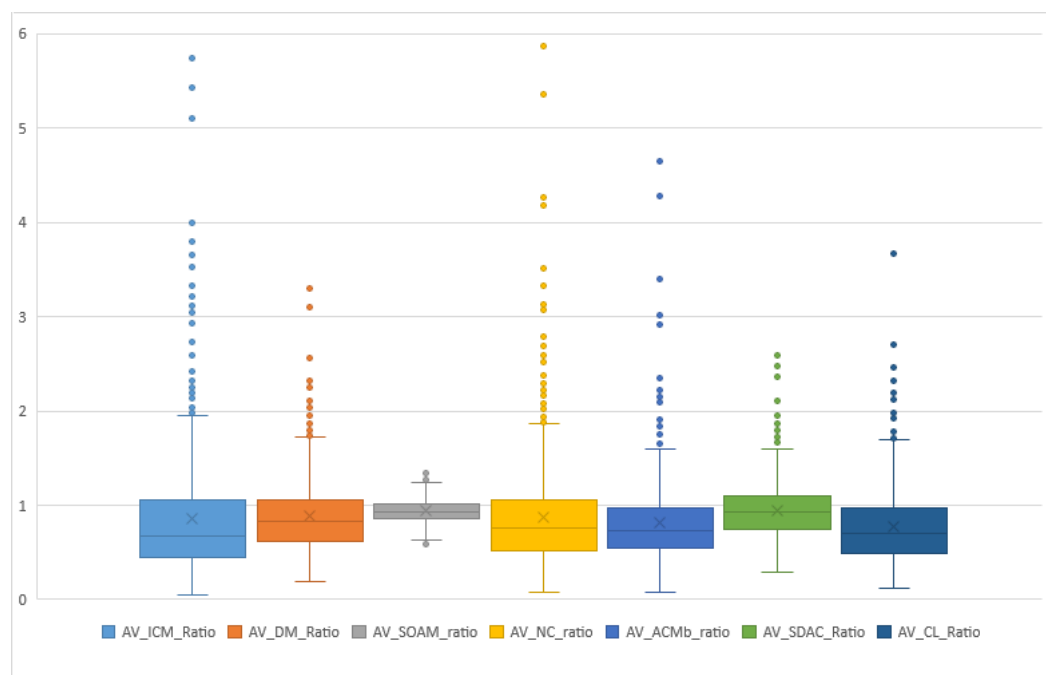


**Figure 13.** Box plots of the generated AV tortuosity metrics ratios of the arteries mean over the veins mean for each image across the AV classification dataset. The AV tortuosity ratios are generated for the metrics ICM, DM, SOAM, NC, ICMb, SDAC, and CL.

#### 4. Discussion

To summarize the findings of this study, fourteen tortuosity measures were analyzed, correlated, discussed, and implemented on 504 images of our AV classification dataset to generate tortuosity metrics image-level and vessel-segment-level feature sets. The image-level feature set was split into arteries and veins feature sets. Statistical methods were applied to the arteries and veins feature sets. Correlation analysis suggests that the most significant observed variables are the ‘Inflection count metric’ and the ‘distance metric’, which correlate with the study’s largest count of other tortuosity metrics. The six tortuosity features, ‘Inflection count metric normal’, ‘Inflection count metric Binomial’, ‘Centerline length’, ‘Norm of curvature’, ‘Distance metric’, and ‘Chord normalized’, were selected based on principal component analysis and correlation analysis.

The linear regression analysis derived the linear relation between the ‘distance metric’ and the five selected metrics. The R-Sq of the generated linear regression formula was 61.6%, which is very low compared to the formulas generated for ICMn that report 89.39% and 89.11% for arteries and veins, respectively. Hence, the ICMn was selected to be the independent variable—the y side of the regression formula. The distance metric was moved to the other side as one of the independent variables in the linear regression formula.

Regression analyses and two sample *T*-tests were carried out to study further the effect of the ‘vessel type’ on the results of quantifying the tortuosity metrics. It was found that the ‘vessel type’ has no significant effect on the tortuosity calculation, as, when applied to the two-sample *T*-test on the veins and arteries feature sets, the *p*-value > 0.05 proved that the null hypothesis in (16) is correct and indicates that the mean of the tortuosity of arteries and the veins are the same. In contrast, the R-Sq values reported in the linear regression analysis for arteries and veins were 89.39% and 89.11%, respectively. This indicates that the linear regression formulas for both arteries and veins represent 89% of the data under study, which are equivalent and strong in both formulas. Hence, the measurement of tortuosity geometric phenomena using ICM is the same for arteries and veins.

The principal component analysis machine learning method was used to identify that ‘inflection count metric normal’ is the most strongly correlated with each compo-

nent/tortuosity metric to finalize the feature selection and the visualization of the linear regression formulas in the 2-dimensional space.

Several experiments were examined using PCA, trying to reach a higher R-Sq value to maximize the linear regression model; as a result, the R-Sq value increased from 83.7% to 89.39% for arteries and from 84.4% to 89.11% for veins. It is worth emphasizing that, in all the experiments, the R-Sq linear regression of two formulas for arteries and veins increase together and remain almost close to each other, indicating that the average of  $ICM_{arteries}$  and the average of  $ICM_{veins}$  are similar.

In this study, we have introduced a new formula that can determine if the tortuosity is in the arteries, veins, or both. Since this quantification is being investigated for the first time, it represents a brand new avenue for research in identifying eye disorders associated with arteries and veins, utilizing retinal image processing. The authors believe that this quantification presents a unique opportunity for future research that will help to create a clear road toward medical application.

In general, we can conclude from analyzing the above arteriovenous length and tortuosity ratios that the findings above are in line with the statistical analysis results that reported that the tortuosity in the arteries is the same for the veins. This study introduces a new concept called AVLR for diagnosing eye vascular changes automatically. This formula is an open area of research in medical image processing and the medical field. It includes the relation between artery/vein tortuosity, which may require further investigation from the medical field. This concept has not been used in the medical field before. The authors are researching the implementation of AVLR on specific regions of interest within the retina for upcoming studies.

The results of this study are applied to classify the AV classification large-scale datasets, which enables making broad generalizations on any set of retinal images. However, to obtain a more specific outcome, it is advisable to incorporate more images from diverse sources, including geographical, age, and gender variations that contain severe diabetic retinopathy or hypertensive retinopathy cases. Further research is required to delve deeper into this study's results to avoid any potential limitations in the results.

## 5. Conclusions

In this work, statistical tests have been performed to test the hypothesis that the tortuosity behavior in the arteries of the retina is the same as in the veins. To prove it, new arteriovenous length ratios are introduced for the first time in the field. The ratios are used to create a feature set to compare the tortuosity in each image while comparing the tortuosity behavior for arteries and veins and proving the hypothesis. Two feature sets are prepared: one for the tortuosity of arteries segments only and the other for the veins segments only, from all the 504 images of the AV classification dataset. The two sample  $T$ -tests and the regression analysis have statistically proven that measuring the tortuosity phenomenon in the fundus images of the eye using ICM is the same for arteries and veins from a geometric point of view. The R-Sq value of the linear regression model has marked the value of 89.11% and 89.39% for veins and arteries results, respectively. The two sample  $T$ -test is used to validate the research claim—the results of the two-sample  $T$ -test = 0.701. As the  $p$ -value  $> 0.05$ , the  $H_0$  research claim is accepted, and hence there is no difference between the arteries' and the veins' average inflection count metric normal (ICMn). If we look at the variations that may happen on the tortuosity at the image level, a set of ratios is introduced that divide the average length of artery segments over the average length of the vein segments, and the result supports the statistical findings with some variations specific to the images. A future area of research is to link the medical literature on retinal vessel tortuosity with the statistical results reached in this study.

**Author Contributions:** The authors have contributed equally to this research. All authors have read and agreed to the published version of the manuscript.

**Funding:** This research received no external funding.

**Data Availability Statement:** Not applicable.

**Acknowledgments:** The Ras Al-Khaimah public library under the umbrella of The UAE Ministry of Culture and Youth, and ‘The American University of Ras Al Khaimah (AURAK)’ are appreciated and thanked by the authors for providing important resources that enabled them to complete this study.

**Conflicts of Interest:** This work was included in the Ph.D. thesis of the first author, which was successfully defended on 27 August 2020. It should be noted that the thesis and its associated source code are safeguarded by copyright law No. 404-2021 in the Ministry of Economics in UAE and 153 other countries.

## Abbreviations

The following abbreviations are used in this manuscript:

|       |   |
|-------|---|
| R-sq  | R Square                                |
| AV    | A for Artery, V for Vein                |
| CRVO  | Central retinal vein occlusion          |
| AVLR  | Arteriovenous length ratio              |
| AVR   | Arteriovenous ratio                     |
| CN    | Chord normalized                        |
| DM    | distance metric                         |
| ICMb  | Inflection count metric Binomial        |
| ICMn  | Inflection count metric normalized      |
| SDavc | Standard deviation of average curvature |
| SOAM  | Sum of Angles metric                    |
| SVM   | Support vector machine                  |
| Navc  | Norm of average curvature               |
| NoC   | Norm of curvature                       |
| PCA   | Principal component analysis            |
| ROP   | Retinopathy of pre-maturity             |
| TSC   | Total squared curvature                 |
| TI    | Tortuosity index                        |

## References

1. Sasongko, M.; Wong, T.; Nguyen, T.; Cheung, C.; Shaw, J.; Wang, J. Retinal vascular tortuosity in persons with diabetes and diabetic retinopathy. *Diabetologia* **2011**, *54*, 2409–2416. [[CrossRef](#)] [[PubMed](#)]
2. Lee, H.; Lee, M.; Chung, H.; Kim, H.C. Quantification of retinal vessel tortuosity in diabetic retinopathy using optical coherence. *Retina* **2018**, *38*, 976–985. [[CrossRef](#)] [[PubMed](#)]
3. Cavallari, M.; Stamile, C.; Umeton, R.; Calimeri, F.; Orzi, F. Novel method for automated analysis of retinal images: Results in subjects with hypertensive retinopathy and CADASIL. *BioMed Res. Int.* **2015**, *2015*, 752957. [[CrossRef](#)] [[PubMed](#)]
4. Dogra, M.; Dogra, M. Congenital tortuous retinal vessels. *Indian J. Ophthalmol.* **2019**, *67*, 277. [[CrossRef](#)] [[PubMed](#)]
5. Cheung, C.Y.; Tay, W.T.; Mitchell, P.; Wang, J.J.; Hsu, W.; Lee, M.L.; Lau, Q.P.; Zhu, A.L.; Klein, R.; Saw, S.M.; et al. Quantitative and qualitative retinal microvascular characteristics and blood pressure. *J. Hypertens.* **2011**, *29*, 1380–1391. [[CrossRef](#)] [[PubMed](#)]
6. Yang, M.B. A pilot study using “roptool” to quantify plus disease in retinopathy of prematurity. *J. Am. Assoc. Pediatr. Ophthalmol. Strabismus* **2007**, *11*, 630–631. [[CrossRef](#)] [[PubMed](#)]
7. Abramoff, M.D.; Garvin, M.K.; Sonka, M. Retinal imaging and image analysis. *IEEE Rev. Biomed. Eng.* **2010**, *3*, 169–208. [[CrossRef](#)] [[PubMed](#)]
8. Del Corso, L.; Moruzzo, D.; Conte, B.; Agelli, M.; Romanelli, A.M.; Pastine, F.; Protti, M.; Pentimone, F.; Baggiani, G. Tortuosity kinking and coiling of the carotid artery: Expression of atherosclerosis or aging? *Angiology* **1998**, *49*, 361–371. [[CrossRef](#)]
9. Ciurică, S.; Lopez-Sublet, M.; Loeys, B.L.; Radhouani, I.; Natarajan, N.; Vikkula, M.; Maas, A.H.; Adlam, D.; Persu, A. Arterial tortuosity: Novel implications for an old phenotype. *Hypertension* **2019**, *73*, 951–960. [[CrossRef](#)]
10. Abdalla, M.; Hunter, A.; Al-Diri, B. Quantifying retinal blood vessels’ tortuosity. In Proceedings of the 2015 Science and Information Conference (SAI), London, UK, 28–30 July 2015; pp. 687–693.
11. Kalitzeos, A.A.; Lip, G.Y.; Heitmar, R. Retinal vessel tortuosity measures and their applications. *Exp. Eye Res.* **2013**, *106*, 40–46. [[CrossRef](#)]
12. Zaki, W.M.D.W.; Zulkifley, M.A.; Hussain, A.; Halim, W.H.W.; Mustafa, N.B.A.; Ting, L.S. Diabetic retinopathy assessment: Towards an automated system. *Biomed. Signal Process. Control* **2016**, *24*, 72–82. [[CrossRef](#)]
13. Lotmar, W.; Freiburghaus, A.; Bracher, D. Measurement of vessel tortuosity on fundus photographs. *Albrecht Von Graefes Arch. FÜR Klin. Und Exp.* **1979**, *211*, 49–57. [[CrossRef](#)]

14. Capowski, J.J.; Kylstra, J.A.; Freedman, S.F. A numeric index based on spatial frequency for the tortuosity of retinal vessels and its application to plus disease in retinopathy of prematurity. *Retina* **1995**, *15*, 490–500. [CrossRef] [PubMed]
15. Heneghan, C.; Flynn, J.; O’Keefe, M.; Cahill, M. characterization of changes in blood vessel width and tortuosity in retinopathy of prematurity using image analysis. *Med. Image Anal.* **2002**, *6*, 407–429. [CrossRef]
16. Gelman, R.; Jiang, L.; Du, Y.E.; Martinez-Perez, M.E.; Flynn, J.T.; Chiang, M.F. Plus disease in retinopathy of prematurity: A pilot study of computer-based and expert diagnosis. *J. Am. Assoc. Pediatr. Ophthalmol. Strabismus* **2007**, *11*, 532–540. [CrossRef] [PubMed]
17. Grisan, E.; Foracchia, M.; Ruggeri, A. A novel method for the automatic grading of retinal vessel tortuosity. *IEEE Trans. Med. Imaging* **2008**, *27*, 310–319. [CrossRef]
18. Kiely, A.E.; Wallace, D.K.; Freedman, S.F.; Zhao, Z. Computer-assisted measurement of retinal vascular width and tortuosity in retinopathy of prematurity. *Arch. Ophthalmol.* **2010**, *128*, 847–852. [CrossRef]
19. Chanrinos, K.; Pilu, M.; Fisher, R.; Trahanias, P. *Image Processing Techniques for the Quantification of Atherosclerotic Changes*; Department of Artificial Intelligence, University of Edinburgh: Edinburgh, UK, 1998.
20. Hart, W.E.; Goldbaum, M.; Côté, B.; Kube, P.; Nelson, M.R. Measurement and classification of retinal vascular tortuosity. *Int. J. Med. Inform.* **1999**, *53*, 239–252. [CrossRef] [PubMed]
21. Dougherty, G.; Varro, J. A quantitative index for the measurement of the tortuosity of blood vessels. *Med. Eng. Phys.* **2000**, *22*, 567–574. [CrossRef] [PubMed]
22. Iorga, M.; Dougherty, G. tortuosity as an indicator of the severity of diabetic retinopathy. In *Medical Image Processing*; Springer: New York, NY, USA, 2011; pp. 269–290.
23. Oloumi, F.; Rangayyan, R.M.; Ells, A.L. Assessment of vessel tortuosity in retinal images of preterm infants. In Proceedings of the 2014 36th Annual International Conference of the IEEE Engineering in Medicine and Biology Society, Chicago, IL, USA, 26–30 August 2014; pp. 5410–5413.
24. Mayrhofer-Reinhartshuber, M.; Cornforth, D.J.; Ahammer, H.; Jelinek, H.F. Multiscale analysis of tortuosity in retinal images using wavelets and fractal methods. *Pattern Recognit. Lett.* **2015**, *68*, 132–138. [CrossRef]
25. Dougherty, G.; Johnson, M.J.; Wiers, M.D. Measurement of retinal vascular tortuosity and its application to retinal pathologies. *Med. Biol. Eng. Comput.* **2010**, *48*, 87–95. [CrossRef] [PubMed]
26. Onkaew, D.; Turior, R.; Uyyanonvara, B.; Akinori, N.; Sinthanayothin, C. Automatic retinal vessel tortuosity measurement using curvature of improved chain code. In Proceedings of the International Conference on Electrical, Control and Computer Engineering 2011 (InECCE), Yichang, China, 16–18 September 2011; pp. 183–186.
27. Turior, R.; Onkaew, D.; Uyyanonvara, B.; Chutinantvarodom, P. Quantification and classification of retinal vessel tortuosity. *Sci. Asia* **2013**, *39*, 265–277. [CrossRef]
28. Chakravarty, A.; Sivaswamy, J. A novel approach for quantification of retinal vessel tortuosity using quadratic polynomial decomposition. In Proceedings of the 2013 Indian Conference on Medical Informatics and Telemedicine (ICMIT), Kharagpur, India, 28–30 March 2013; pp. 7–12.
29. Wilson, C.M.; Cocker, K.D.; Moseley, M.J.; Paterson, C.; Clay, S.T.; Schulenburg, W.E.; Mills, M.D.; Ells, A.L.; Parker, K.H.; Quinn, G.E.; et al. Computerized analysis of retinal vessel width and tortuosity in premature infants. *Investig. Ophthalmol. Vis. Sci.* **2008**, *49*, 3577–3585. [CrossRef] [PubMed]
30. Narasimhan, K.; Vijayarekha, K. Automated diagnosis of hypertensive retinopathy using fundus images. *Res. J. Pharm. Technol.* **2015**, *8*, 1534. [CrossRef]
31. Badawi, S.A.; Fraz, M.M. Optimizing the trainable b-cosfire filter for retinal blood vessel segmentation. *PeerJ* **2018**, *6*, e5855. [CrossRef] [PubMed]
32. Badawi, S.A.; Fraz, M.M. Multiloss function based deep convolutional neural network for segmentation of retinal vasculature into arterioles and venules. *BioMed Res. Int.* **2019**, *2019*, 4747230. [CrossRef] [PubMed]
33. Badawi, S.A.; Takruri, M.; ElBadawi, I.; Chaudhry, I.A.; Mahar, N.U.; Nileshwar, A.K.; Mosalam, E. Enhancing Vessel Segment Extraction in Retinal Fundus Images Using Retinal Image Analysis and Six Sigma Process Capability Index. *Mathematics* **2023**, *11*, 3170. [CrossRef]
34. Bullitt, E.; Gerig, G.; Pizer, S.M.; Lin, W.; Aylward, S.R. Measuring tortuosity of the intracerebral vasculature from MRA images. *IEEE Trans. Med. Imaging* **2003**, *22*, 1163–1171. [CrossRef]
35. Puth, M.-T.; Neuhäuser, M.; Ruxton, G.D. Pearson Product-Moment Correlation Coefficient. 2014. Available online: <https://statistics.laerd.com/statistical-guides/pearson-correlation-coefficient-statistical-guide.php> (accessed on 10 September 2019).
36. Chee, J. *Pearson’s Product Moment Correlation: Sample Analysis*; University of Hawaii at Mānoa School of Nursing: Honolulu, HI, USA, 2015; Volume 4, pp. 4–90.
37. Cressie, N.A.C.; Whitford, H.J. How to use the two sample t-test. *Biom. J.* **1986**, *28*, 131–148. [CrossRef]
38. Meyer, R.; Krueger, D. *MINITAB Guide to Statistics*; Prentice-Hall, Inc.: Upper Saddle River, NJ, USA, 1997.

**Disclaimer/Publisher’s Note:** The statements, opinions and data contained in all publications are solely those of the individual author(s) and contributor(s) and not of MDPI and/or the editor(s). MDPI and/or the editor(s) disclaim responsibility for any injury to people or property resulting from any ideas, methods, instructions or products referred to in the content.